한국소음진동공학회지 제 10 권 제 3 호, pp. 536~550, 2000.

〈논 문〉

Modal Analysis of Eccentric Shells with Fluid-Filled Annulus

유체가 채워진 환형공간을 갖는 편심 원통형 셸의 모드 해석

Myung Jo Jhung*, Kyeong Hoon Jeong** and Youn Won Park***
정 명 조 · 정 경 훈 · 박 윤 원

(2000년 3월 20일 접수 ; 2000년 5월 13일 심사완료)

Key Words : Cylindrical Shell(실린더형 셸), Modal Characteristic(모드 특성), Fluid-Filled Annulus(유체가 채워진 환형공간), Finite Element Method(유한요소법), Eccentricity(편심률)

ABSTRACT

Investigated in this study are the modal characteristics of the eccentric cylindrical shells with fluid-filled annulus. Theoretical method is developed to find the natural frequencies of the shell using the finite Fourier expansion, and their results are compared with those of finite element method to verify the validation of the method developed. The effect of eccentricity on the modal characteristics of the shells is investigated using a finite element modeling.

요 약

본 연구에서는 유체가 채워진 환형공간을 갖는 편심 원통형 셸의 모드 특성을 조사하였다. Stokes 변환을 응용한 Fourier 급수전개법으로 고유진동수를 구하는 방법을 전개하여 유체가 채워진 환형공간을 갖는 편심 원통형 셸에 대한 이론적인 해를 구하였고 이를 유한요소법에 의한 값과 비교하였다. 또한 편심된 정도가 원통형 셸의 모드 특성에 미치는 영향을 검토하였고 편심율에 따른 이들의 특성도 고찰하였다.

1. Introduction

A fluid-surrounded cylindrical shells subjected to various loads have been widely used as structural components in the engineering design. One example is reactor internals such as core barrel and upper structure barrel coupled with each other by fluid-filled annulus[1]. To assure the reliability of those components and to verify structural integrity during normal operations of a nuclear power plant[2], it is necessary to investigate extensively flow-induced vibration, necessitating the investigation of the modal characteristics. Several monitoring systems such as internal vibration monitoring system using neutron noise analysis are employed to find in advance the defect which may cause severe damage on the reactor internals and steam generator and to take actions to prevent such damage in time. One of major causes for accidents is the eccentricity of inner shell when it is submerged in a fluid which came from the failure of connections to other major components

Several previous investigations have been performed to

* 정회원, 한국원자력안전기술원, 방사선공학연구실
* 정회원, 한국원자력연구소, 동력로기술개발팀
* 한국원자력안전기술원, 방사선공학연구실

analyze the free vibration of fluid-filled, coaxial cylindrical shells[3, 4], which were limited to the approximated methods and could provide only the in-phase and out-of-phase modes of coaxial shells with small annular fluid gap compared to the shell diameters. Therefore, an advanced general theory was developed to calculate the natural frequencies for all vibrational modes of two coaxial circular cylindrical shells coupled with fluid[5]. Even though coaxial shells are extensively studied very few studies of eccentric shells are found. Danila et al.[6] suggested a calculating method of the scattered field due to a plane wave incident on one or several cylindrical fluid-fluid interfaces using the generalized Debye series expansion. The theoretical method is applied to a concentric and a non-concentric fluid shell and then extended to the multi-layered cylindrical structure. However, few theoretical studies on the free vibration of a circular cylindrical shell submerged in a compressible fluid-filled cylindrical container were taken into consideration.

This study develops an advanced general theory to calculate the natural frequencies for all vibrational modes of two eccentric circular cylindrical shells with fluid-filled annulus. To support the validity of the proposed theory, finite element analyses are carried out for various eccentricities. The effect of eccentricity on the natural frequencies of the shells is investigated by comparing frequencies according to the eccentricity.

2. Theory

2.1 Equation of Motion

Consider a circular cylindrical shell with a clamped boundary condition at both ends, as illustrated in Fig. 1. The shell can be concentrically or eccentrically submerged in a fluid-filled container. The cylindrical shell has mean radius R, height L, and wall thickness h. The Sanders' shell equations[7, 8] as the governing equations for the shell where the hydrodynamic effects are considered, can be written as :

$$R^2 u_{,xy} + \frac{(1-\mu)}{2}\left(1+\frac{k}{4}\right)u_{,\theta\theta} + R\left\{\frac{(1-\mu)}{2} - \frac{3(1-mi)}{8}k\right\}v_{,x\theta} + \mu R w_{,x} + \frac{(1-\mu)}{2}Rkw_{,x\theta} = \gamma^2 u_{,u} \quad (1a)$$

$$R\left\{\frac{(1-\mu)}{2} - \frac{3(1-\mu)}{8}k\right\}u_{,x\theta} + (1+k)v_{,\theta\theta} + \frac{(1-\mu)}{2}R^2\left(1+\frac{9k}{4}\right)v_{,xx} - \frac{(3-\mu)}{2}R^2 k\, w_{,xx\theta} + w_{,\theta} - k\, w_{,\theta\theta\theta} = \gamma^2 v_{,tt} \quad (1b)$$

$$\frac{(1-\mu)}{2}Rk\,u_{,x\theta} + \mu R u_{,x} - \frac{(3-k)}{2}R^2 k\, v_{,xx\theta} + v_{,\theta} + w + k\left(R^4 w_{,xxxx} + 2R^2 w_{,xx\theta\theta} + w_{,\theta\theta\theta\theta} - v_{,\theta\theta\theta}\right) = -\gamma^2 u_{,tt} + \frac{R^2 p}{D} \quad (1c)$$

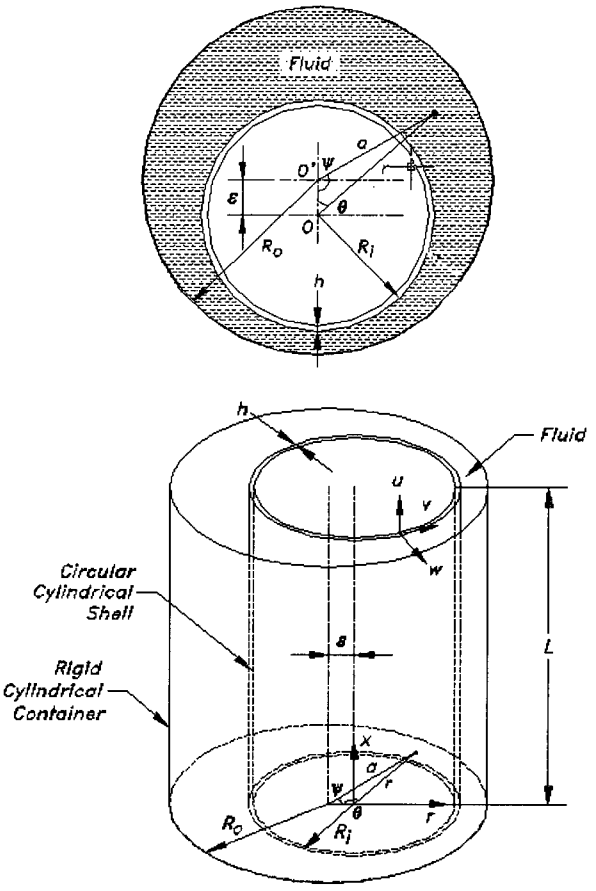

Fig. 1 Eccentric cylindrical shells with fluid-filled annulus

The comma in the equations denotes a partial derivative with respect to the corresponding variable. For a complete description of the shell motions, it is necessary to add boundary conditions to the equations of motion. Consider the simplest end arrangements of the shell on the top and bottom supports. At both ends of a concentrically or eccentrically arranged shell with respect

to a rigid circular cylindrical container, all the boundary conditions will obviously hold for the case of SCC (Sine-Cosine-Cosine) formulation [9]:

for the bottom support of the shell,

$$M_x(0) = N_x(0) = v(0) = w(0) = 0, \tag{2a}$$

for the top support of the shell,

$$M_x(L) = N_x(L) = v(L) = w(L) = 0, \tag{2b}$$

where M_x and N_x denote the bending moment and the membrane tensile force, respectively. All geometric boundary conditions applicable to the clamped-clamped shell can be reduced to the following equations for the ends of the shell[10]:

$$v(0) = w(0) = v(L) = w(L) = 0. \tag{3}$$

The relationships between the boundary forces and displacements are

$$N_x = D\left[u_{,x} + \frac{\mu}{R}v_{,\theta} + \frac{\mu}{R}w\right], \tag{4a}$$

$$N_{x\theta} = \frac{D(1-\mu)}{2}\left[\frac{1}{R}\left(1-\frac{3}{4}k\right)u_{,\theta} + \left(1+\frac{9}{4}k\right)v_{,x} - 3k\,w_{,x\theta}\right], \tag{4b}$$

$$Q_x = K\left[-\frac{(1-\mu)}{2R^3}u_{,\theta\theta} + \frac{(3-\mu)}{2R^2}v_{,x\theta} - \frac{(2-\mu)}{R^2}w_{,x\theta\theta} - w_{,xxx}\right] \tag{4c}$$

$$M_x = K\left[\frac{\mu}{R^2}(v_{,\theta} - w_{,\theta\theta}) - w_{,xx}\right] \tag{4d}$$

where $D = Eh/(1-\mu^2), K = Eh^3/12(1-\mu^2), k = h^2/12R^2$. $N_{x\theta}$ and Q_x denote the membrane shear force and transverse shear force per unit length, respectively.

2.2 Modal Functions

A general relation for the dynamic displacements in any vibration mode of the shell can be written in the following form for the cylindrical coordinate r, q.

$$u(x,\theta,t) = u(x,\theta)\exp(iwt), \tag{5a}$$

$$v(x,\theta,t) = v(x,\theta)\exp(iwt), \tag{5b}$$

$$w(x,\theta) = w(x,\theta)\exp(iwt); \tag{5c}$$

where $u(x,\theta)$, $v(x,\theta)$, and $w(x,\theta)$ are modal functions corresponding to the axial, tangential, and radial displacements for the shell, respectively. These modal functions along the axial direction can be described by a sum of linear combinations of the Fourier series that are orthogonal.

$$u(x,\theta) = \sum_{n=1}^{\infty}\sum_{s=1}^{\infty} A_{sn}\sin\left(\frac{s\pi x}{L}\right)\cos n\theta, \tag{6a}$$

$$v(x,\theta) = \sum_{n=1}^{\infty}\left[B_{on} + \sum_{s=1}^{\infty} B_{sn}\cos\left(\frac{s\pi x}{L}\right)\right]\sin n\theta, \tag{6b}$$

$$w(x,\theta) = \sum_{n=1}^{\infty}\left[C_{on} + \sum_{s=1}^{\infty} C_{sn}\cos\left(\frac{s\pi x}{L}\right)\right]\cos n\theta. \tag{6c}$$

The derivatives of the above modal functions for the shell can be obtained using the finite Fourier transformation[10, 11]. The modal functions and their derivatives of the cylindrical shell were described in reference[10].

2.3 Equation of Fluid Motion

The inviscid, irrotational and compressible fluid movement due to shell vibration is described by the Helmholz equation :

$$\Phi_{,rr} + \frac{1}{r}\Phi_{,r} + \frac{1}{r^2}\Phi_{,\theta\theta} + \Phi_{,xx} = \frac{1}{c^2}\Phi_{,tt} \quad ; \tag{7}$$

where c is the speed of sound in the fluid medium equal to $\sqrt{B/\rho_0}$. B is the bulk modulus of elasticity of fluid and ρ_0 stands for the fluid density. It is possible to separate the function Φ with respect to x by observing that, in the axial direction, the rigid surfaces support the edges of the shell; thus

$$\Phi(x,r,\theta,t) = i\omega\phi(r,\theta,x)\exp(i\omega t) = i\omega\eta(r,\theta)f(x)\exp(i\omega t) \quad ; \tag{8}$$

where ω is the fluid-coupled frequency of the shell. Substitution of equation (8) into the partial differential equation (7) gives

$$\frac{\eta(r,\theta)_{,rr} + \frac{1}{r}\eta(r,\theta)_{,r} + \frac{1}{r^2}\eta(r,\theta)_{,\theta\theta} + \left(\frac{\omega}{c}\right)^2\eta(r,\theta)}{\eta(r,\theta)} = -\frac{f(x)_{,xx}}{f(x)} = \left(\frac{s\pi}{L}\right)^2, \tag{9}$$

It is possible to solve the partial differential equation (9) by the separation of the variables. The solution can

be obtained with respect to the original cylindrical coordinates, r, θ and x:

for $\frac{s\pi}{L} \geq \frac{\omega}{c}$,

$$\phi(r,\theta,x)=\sum_{n=1}^{\infty}\left[\begin{array}{l} D_{on}\,J_n\left(\frac{\omega r}{c}\right)+F_{on}\,Y_n\left(\frac{\omega r}{c}\right) \\ +\sum_{s=1}^{\infty}\{D_{sn}\,I_n(\alpha_{sn}r)+F_{sn}\,K_n(\alpha_{sn}r)\}\cos\left(\frac{s\pi x}{L}\right)\end{array}\right]\sin n\theta \tag{10a}$$

and for $\frac{s\pi}{L} < \frac{\omega}{c}$

$$\phi(r,\theta,x)=\sum_{n=1}^{\infty}\left[\begin{array}{l} D_{on}\,J_n\left(\frac{\omega r}{c}\right)+F_{on}\,Y_n\left(\frac{\omega r}{c}\right) \\ +\sum_{s=1}^{\infty}\{D_{sn}\,J_n(\alpha_{sn}r)+F_{sn}\,Y_n(\alpha_{sn}r)\}\cos\left(\frac{s\pi x}{L}\right)\end{array}\right]\sin n\theta \tag{10b}$$

where J_n and Y_n are Bessel functions of the first and second kinds of order n, whereas In and K_n are modified Bessel functions of the first and second kinds of order n. ψ means the spatial velocity potential of the contained compressible fluid. α_{sn} is related to the speed of sound in the fluid medium as follows :

$$\alpha_{sn}=\sqrt{\left|\left(\frac{s\pi}{L}\right)^2-\left(\frac{\omega}{c}\right)^2\right|} \quad \text{for } s = 1, 2, 3, \ldots. \tag{11}$$

The equations (10a) and (10b) automatically satisfy the boundary conditions that appear as follows:

(a) impermeable rigid surface on the bottom is

$$\frac{\partial\phi(r,\theta,x)}{\partial x}=0 \qquad \text{at} \;:\; x=0 \tag{12}$$

(b) as there exists no free surface, the axial fluid velocity at the rigid top is also zero, so

$$\frac{\partial\phi(r,\theta,x)}{\partial x}=0 \qquad \text{at} \quad x=L. \tag{13}$$

2.4 General Formulation

For the eccentrically submerged shell, the velocity potential of equations (10a) and (10b) can be transformed to the shifted cylindrical coordinates, (a, Ψ, x) by Graf's addition theorem and Beltrami's theorem [12]:

for $\frac{s\pi}{L} \geq \frac{\omega}{c}$,

$$\phi(a,\psi,x)=\sum_{n=1}^{\infty}\sum_{m=-\infty}^{\infty}\left[\begin{array}{l} \left\{D_{on}\,J_{n+m}\left(\frac{\omega a}{c}\right)+F_{on}\,Y_{n+m}\left(\frac{\omega a}{c}\right)\right\}J_m\left(\frac{\omega\varepsilon}{c}\right) \\ +\sum_{s=1}^{\infty}\left\{D_{sn}(-1)^m I_{n+m}(\alpha_{sn}a)+F_{sn}K_{n+m}(\alpha_{sn}a)\right\} \\ \times I_m(\alpha_{sn}\varepsilon)\cos\left(\frac{s\pi x}{L}\right)\end{array}\right]\sin m\psi \tag{14a}$$

for $\frac{s\pi}{L} < \frac{\omega}{c}$,

$$\phi(a,\psi,x)=\sum_{n=1}^{\infty}\sum_{m=-\infty}^{\infty}\left[\begin{array}{l} \left\{D_{on}\,J_{n+m}\left(\frac{\omega a}{c}\right)+F_{on}\,Y_{n+m}\left(\frac{\omega a}{c}\right)\right\}J_m\left(\frac{\omega\varepsilon}{c}\right) \\ +\sum_{s=1}^{\infty}\{D_{sn}\,J_{n+m}(\alpha_{sn}a)+F_{sn}\,Y_{n+m}(\alpha_{sn}a)\} \\ \times J_m(\alpha_{sn}\varepsilon)\cos\left(\frac{s\pi x}{L}\right)\end{array}\right]\sin m\psi \tag{14b}$$

It is convenient to handle the boundary condition along the surface of the rigid container when the velocity potential is transformed from the origin "O" to the shifted origin "O'". The radial fluid velocity along the outer wetted surface of the shell must be identical to that of the flexible shell, so

$$\frac{\partial\phi(r,\theta,x)}{\partial r}=-w(x,\theta) \qquad \text{at} \;.\, r=R \tag{15}$$

Additionally, the radial fluid velocity along the wetted surface of the outer rigid container that maintains eccentricity to the shell must be zero, so

$$\frac{\partial\phi(x,\psi,a)}{\partial a}=0 \qquad \text{at} \quad a=R_0, \tag{16}$$

Substitution of equations (6c), (14a) and (14b) into equations (15) and (16) gives the relationships:

for $\frac{s\pi}{L} \geq \frac{\omega}{c}$,

$$\sum_{n=1}^{\infty}\left[\begin{array}{l} \left(\frac{\omega}{c}\right)\left\{D_{on}\,J_n'\left(\frac{\omega R}{c}\right)+F_{on}\,Y_n'\left(\frac{\omega R}{c}\right)\right\} \\ +\sum_{s=1}^{\infty}\alpha_{sn}\{D_{sn}\,I_n'(\alpha_{sn}R)+F_{sn}\,K_n'(\alpha_{sn}R)\}\cos\left(\frac{s\pi x}{L}\right)\end{array}\right]\cos n\theta$$

$$= -\sum_{n=1}^{\infty}\left[C_{on} + \sum_{s=1}^{\infty} C_{sn}\cos\left(\frac{s\pi x}{L}\right)\right]\cos n\theta \tag{17a}$$

for $\frac{s\pi}{L} < \frac{\omega}{c}$,

$$\sum_{n=1}^{\infty}\left[\begin{array}{l}\left(\frac{\omega}{c}\right)\left\{D_{on}J_n'\left(\frac{\omega R}{c}\right)+F_{on}Y_n'\left(\frac{\omega R}{c}\right)\right\} \\ +\sum_{s=1}^{\infty}\alpha_{sn}\{D_{sn}J_n'(\alpha_{sn}R)+F_{sn}Y_n'(\alpha_{sn}R)\}\cos\left(\frac{s\pi x}{L}\right)\end{array}\right]\cos n\theta$$

$$= -\sum_{n=1}^{\infty}\left[C_{on} + \sum_{s=1}^{\infty} C_{sn}\cos\left(\frac{s\pi x}{L}\right)\right]\cos n\theta \tag{17b}$$

for $\frac{s\pi}{L} \geq \frac{\omega}{c}$,

$$\sum_{m=-\infty}^{\infty}\left[\begin{array}{l}\left(\frac{\omega}{c}\right)J_m\left(\frac{\omega\varepsilon}{c}\right)\left\{D_{on}J_{n+m}'\left(\frac{\omega R_o}{c}\right)+F_{on}Y_{n+m}'\left(\frac{\omega R_o}{c}\right)\right\} \\ +\sum_{s=1}^{\infty}\alpha_{sn}I_m(\alpha_{sn}\varepsilon)\{D_{sn}(-1)^m I_{n+m}'(\alpha_{sn}R_o)+F_{sn}K_{n+m}'(\alpha_{sn}R_o)\} \\ \times\cos\left(\frac{s\pi x}{L}\right)\end{array}\right] = 0 \tag{18a}$$

for $\frac{s\pi}{L} < \frac{\omega}{c}$,

$$\sum_{m=-\infty}^{\infty}\left[\begin{array}{l}\left(\frac{\omega}{c}\right)J_m\left(\frac{\omega\varepsilon}{c}\right)\left\{D_{on}J_{n+m}'\left(\frac{\omega R_o}{c}\right)+F_{on}Y_{n+m}'\left(\frac{\omega R_o}{c}\right)\right\} \\ +\sum_{s=1}^{\infty}\alpha_{sn}J_m(\alpha_{sn}\varepsilon)\{D_{sn}J_{n+m}'(\alpha_{sn}R_o)+F_{sn}Y_{n+m}'(\alpha_{sn}R_o)\} \\ \times\cos\left(\frac{s\pi x}{L}\right)\end{array}\right] = 0 \tag{18b}$$

Now, all unknown coefficients D_{on}, F_{on}, D_{sn} and F_{sn} related to the fluid motion will be written in terms of the coefficients C_{on} and C_{sn} related to the shell motion using equations (17a), (17b), (18a) and (18b).

$$F_{on} = W_{n1}D_{on}, \tag{19a}$$

$$D_{on} = \Gamma_{n1}C_{on}, \tag{19b}$$

$$F_{on} = \Gamma_{n2}C_{on}: \tag{19c}$$

For $\frac{s\pi}{L} \geq \frac{\omega}{c}$,

$$F_{sn} = W_{n2}D_{sn}, \tag{19d}$$

$$D_{sn} = \Gamma_{sn3}C_{sn}, \tag{19e}$$

$$F_{sn} = \Gamma_{sn5}C_{sn}; \tag{19f}$$

For $\frac{s\pi}{L} < \frac{\omega}{c}$,

$$F_{sn} = W_{n3}D_{sn}, \tag{19g}$$

$$D_{sn} = \Gamma_{sn4}C_{sn}, \tag{19h}$$

$$F_{sn} = \Gamma_{sn6}C_{sn}; \tag{19i}$$

where

$$W_{n1} = -\frac{\sum_{m=-\infty}^{\infty}\left\{J_m\left(\frac{\omega\varepsilon}{c}\right)J_{n+m}'\left(\frac{\omega R_o}{c}\right)\right\}}{\sum_{m=-\infty}^{\infty}\left\{J_m\left(\frac{\omega\varepsilon}{c}\right)Y_{n+m}'\left(\frac{\omega R_o}{c}\right)\right\}}, \tag{20a}$$

$$W_{n2} = -\frac{\sum_{m=-\infty}^{\infty}\{I_m(\alpha_{sn}\varepsilon)(-1)^m I_{n+m}'(\alpha_{sn}R_o)\}}{\sum_{m=-\infty}^{\infty}\{I_m(\alpha_{sn}\varepsilon)K_{n+m}'(\alpha_{sn}R_o)\}}, \tag{20b}$$

$$W_{n3} = -\frac{\sum_{m=-\infty}^{\infty}\{J_m(\alpha_{sn}\varepsilon)J_{n+m}'(\alpha_{sn}R_o)\}}{\sum_{m=-\infty}^{\infty}\{J_m'(\alpha_{sn}\varepsilon)Y_{n+m}'(\alpha_{sn}R_o)\}}, \tag{20c}$$

$$\Gamma_{n1} = -\left(\frac{c}{\omega}\right)\left[J_n'\left(\frac{\omega R}{c}\right)+W_{n1}Y_n'\left(\frac{\omega R}{c}\right)\right]^{-1}, \tag{20d}$$

$$\Gamma_{n2} = W_{n1}\Gamma_{n1}, \tag{20e}$$

$$\Gamma_{sn3} = \frac{-1}{\alpha_{sn}[I_n'(\alpha_{sn}R)+W_{n2}K_n'(\alpha_{sn}R)]}, \tag{20f}$$

$$\Gamma_{sn4} = \frac{-1}{\alpha_{sn}[J_n'(\alpha_{sn}R)+W_{n3}Y_n'(\alpha_{sn}R)]}, \tag{20g}$$

$$\Gamma_{sn5} = W_{n2}\Gamma_{sn3}, \tag{20h}$$

$$\Gamma_{sn6} = W_{n3}\Gamma_{sn4}. \tag{20i}$$

As the eccentric distance e approaches zero, $J_m(\alpha_{sn}\varepsilon)$ and $I_m(\alpha_{sn}\varepsilon)$ of equation (20a) ~ (20c) will be zero for $m \neq 0$ and $J_m(\alpha_{sn}\varepsilon) = I_m(\alpha_{sn}\varepsilon) = 1$ for $m = 0$. Therefore, when $\varepsilon = 0$, equation (20) for the eccentric arrangement of the shell obviously reduces to the equation of the concentric case. The concentrically submerged shell will be a special case of the shell submerged eccentrically in a fluid-filled container.

When the hydrostatic pressure on the shell are neglected for simple formulation, the hydrodynamic pressure along the outer wetted shell surface can be given by

$$p(x,\theta,t)=\rho_o\omega^2\phi(R,\theta,x)\exp(i\omega t), \tag{21}$$

Finally, the hydrodynamic force on the shell can be written as

for $\frac{s\pi}{L}\geq\frac{\omega}{c}$,

$$\frac{R^2\,p(x,\theta,t)}{D}=\frac{\rho_o\omega^2R^2}{D}\sum_{n=1}^{\infty}\left[\begin{array}{l}C_{on}\left\{\Gamma_{n1}J_n\left(\frac{\omega R}{c}\right)+\Gamma_{n2}Y_n\left(\frac{\omega R}{c}\right)\right\}\\+\sum_{s=1}^{\infty}C_{sn}\{\Gamma_{sn3}I_n(\alpha_{sn}R)+\Gamma_{sn5}K_n(\alpha_{sn}R)\}\end{array}\right]\exp(i\omega t) \tag{22a}$$

for $\frac{s\pi}{L}<\frac{\omega}{c}$,

$$\frac{R^2\,p(x,\theta,t)}{D}=\frac{\rho_o\omega^2R^2}{D}\sum_{n=1}^{\infty}\left[\begin{array}{l}C_{on}\left\{\Gamma_{n1}J_n\left(\frac{\omega R}{c}\right)+\Gamma_{n2}Y_n\left(\frac{\omega R}{c}\right)\right\}\\+\sum_{s=1}^{\infty}C_{sn}\{\Gamma_{sn4}J_n(\alpha_{sn}R)+\Gamma_{sn6}Y_n(\alpha_{sn}R)\}\end{array}\right]\exp(i\omega t) \tag{22b}$$

The dynamic displacements and their derivatives can be represented by a Fourier sine and cosine series in an open range of $0<x<L$ and with the end values using the finite Fourier transformation(11). Substitution of the displacements and their derivatives into the governing Sanders' shell equation (1a), (1b) and (1c), leads to an explicit relation for Con and a set of equations for A_{sn}, B_{sn} and C_{sn} as follows :

$$\begin{bmatrix}B_{on}\\C_{on}\end{bmatrix}=\mathbf{y}_1[u_o+u_l]+\mathbf{y}_2[v_o+v_l]+\mathbf{y}_3[\tilde{w}_o+\tilde{w}_l]+\mathbf{y}_4[\tilde{\tilde{w}}_o+\tilde{\tilde{w}}_l], \tag{23}$$

$$\begin{bmatrix}A_{sn}\\B_{sn}\\C_{sn}\end{bmatrix}=\mathbf{y}_5[u_o+(-1)^m u_l]+\mathbf{y}_6[v_o+(-1)^m v_l]+\mathbf{y}_7[\tilde{w}_o+(-1)^m\tilde{w}_l]+\mathbf{y}_8[\tilde{\tilde{w}}_o+(-1)^m\tilde{\tilde{w}}_l] \tag{24}$$

where the end values u_0, u_1, v_0, v_1, $\tilde{w}_0$, $\tilde{w}_1$, $\tilde{\tilde{w}}_0$, and $\tilde{\tilde{w}}_1$ in equations (23) and (24) are defined in reference[10]. The matrix $\mathbf{y}_1$, $\mathbf{y}_2$, ···, $\mathbf{y}_8$ are the derived column matrices. The equivalent hydrodynamic mass effect on the shell is included in the coefficient. The forces $N_{x\theta}$ and Q_x at the ends of the shells can be written as a combination of some boundary values of displacement and their derivatives using equation (4). The boundary values of displacement and their derivatives, v_0, v_1, $\tilde{\tilde{w}}_0$, and $\tilde{\tilde{w}}_1$ can be transformed in a combination of the boundary values of u, $\tilde{w}$, $N_{x\theta}$ and Q_x by equation (4), as written in the form

$$v_o=g_1u_o+g_2\tilde{w}_o+g_3N^o_{x\theta}, \tag{25a}$$

$$v_l=g_1u_l+g_2\tilde{w}_l+g_3N^l_{x\theta}, \tag{25b}$$

$$\tilde{\tilde{w}}_o=g_4u_o+g_5\tilde{w}_o+g_6N^o_{x\theta}+g_7Q^o_x, \tag{25c}$$

$$\tilde{\tilde{w}}_l=g_4u_l+g_5\tilde{w}_l+g_6N^l_{x\theta}+g_7Q^l_x; \tag{25d}$$

where the end values of the forces are defined in reference(10) and gk (k = 1, 2, ... , 7) can be derived. Substitution of equation (25) into equations (23) and (24), gives

$$\begin{bmatrix}B_{on}\\C_{on}\end{bmatrix}=\mathbf{z}_1[u_o+u_l]+\mathbf{z}_2[\tilde{w}_o+\tilde{w}_l]+\mathbf{z}_3[N^o_{x\theta}+N^l_{x\theta}]+\mathbf{z}_4[Q^o_x+Q^l_x], \tag{26a}$$

$$\begin{bmatrix}A_{sn}\\B_{sn}\\C_{sn}\end{bmatrix}=[\Lambda_{ik}]\begin{bmatrix}u_o+(-1)^m u_l\\\tilde{w}_o+(-1)^m\tilde{w}_l\\N^o_{x\theta}+(-1)^m N^l_{x\theta}\\Q^o_x+(-1)^m Q^l_x\end{bmatrix}. \tag{26b}$$

where z_k (k=1,2,3,4) in equation (26a) are the derived coefficient matrices, and $[\Lambda_{ik}]$ (i = 1, 2, 3 and k = 1, 2, 3, 4) in equation (26b) is the 4 × 3 derived coefficients matrix. Eventually, all Fourier coefficients A_{sn}, B_{sn} and C_{sn} are rearranged with a combination of the end point values, as shown in equation (26b).

The geometric boundary conditions that must be satisfied are associated with the dynamic displacement v and w as described in equation (3). Hence it follows that

$$v(0)=\sum_{n=1}^{\infty}\left[B_{on}+\sum_{s=1}^{\infty}B_{sn}\right]=0, \tag{27a}$$

$$v(L)=\sum_{n=1}^{\infty}\left[B_{on}+\sum_{s=1}^{\infty}B_{sn}(-1)^m\right]=0, \tag{27b}$$

$$w(0)=\sum_{n=1}^{\infty}\left[C_{on}+\sum_{s=1}^{\infty}C_{sn}\right]=0, \tag{27c}$$

$$w(L)=\sum_{n=1}^{\infty}\left[B_{on}+\sum_{s=1}^{\infty}B_{sn}(-1)^m\right]=0. \tag{27d}$$

Substitution of equation (26) for the coefficients B_{on},

C_{on}, A_{sn}, B_{sn}, and C_{sn} into the four constraint conditions that come from the geometric boundary condition, written as equation (27), leads to a homogeneous matrix equation by omitting the details :

$$\begin{bmatrix} e_{11} & e_{12} & e_{13} & e_{14} & e_{15} & e_{16} & e_{17} & e_{18} \\ e_{21} & e_{22} & e_{23} & e_{24} & e_{25} & e_{26} & e_{27} & e_{28} \\ e_{31} & e_{32} & e_{33} & e_{34} & e_{35} & e_{36} & e_{37} & e_{38} \\ e_{41} & e_{42} & e_{43} & e_{44} & e_{45} & e_{46} & e_{47} & e_{48} \end{bmatrix} \begin{Bmatrix} u_o \\ u_l \\ \tilde{w}_o \\ \tilde{w}_l \\ N^o_{x\theta} \\ N^l_{x\theta} \\ Q^o_x \\ Q^l_x \end{Bmatrix} = \{0\} \quad (28)$$

The elements of the matrix, e_{ik} (i = 1, 2, 3, 4 and k = 1, 2, ... 8) can be obtained from equation (27). However, when the cylindrical shell is clamped at both support ends, the associated boundary condition is

$$u = v = w = w,_x = 0 \text{ at } x = 0 \text{ and } L. \quad (29)$$

Among these boundary conditions, the two geometric boundary conditions $u = 0$ and $\tilde{w}_0 = 0$ at $x = 0$ and $x = L$ are not automatically satisfied by equation (6), the modal functions set. Therefore the first, second, third, and fourth rows of the matrix in equation (28) are enforced and the terms associated with u_0, u_1, $\tilde{w}_0$, and $\tilde{w}_1$ are released. The 4×4 frequency determinant is obtained from equations (28) and (29) by retaining the rows and columns associated with $N^0_{x\theta}$, $N^l_{x\theta}$, Q^0_x, and Q^1_x. For the clamped boundary condition, the coupled natural frequencies are numerically obtained from the frequency determinant :

$$\begin{vmatrix} e_{15} & e_{16} & e_{17} & e_{18} \\ e_{25} & e_{26} & e_{27} & e_{28} \\ e_{35} & e_{36} & e_{37} & e_{38} \\ e_{45} & e_{46} & e_{47} & e_{48} \end{vmatrix} = 0 \quad (30)$$

3. Analysis

3.1 Theoretical Analysis

On the basis of the preceding analysis, the frequency determinant is numerically solved for the clamped boundary condition in order to find the natural frequencies of the eccentric circular cylindrical shells with a fluid-filled annulus. The inner and outer shells are coupled with a fluid-filled annular gap. The inner cylindrical shell has a mean radius of 100 mm, a length of 300 mm, and a wall thickness of 2 mm. The outer cylindrical shell has a mean radius of 130 mm with the same length and wall thickness. The physical properties of the shell material are as follows: Young's modulus = 69.0 GPa, Poisson's ratio = 0.3, and mass density = 2700 kg/m^3. Water is used as the contained fluid with a density of 1000 kg/m^3. The sound speed in water, 1483 m/s, is equivalent to the bulk modulus of elasticity, 2.2 GPa. Dimensions and material properties used for the analysis are shown in Table 1.

The frequency equation derived in the preceding section involves the double infinite series of algebraic terms. Before exploring the analytical method for obtaining the natural frequencies of the fluid-coupled shells, it is necessary to conduct convergence studies and establish the number of terms required in the series expansions involved. In the numerical calculation, the Fourier expansion term m is set at 100, which gives an exact enough solution by convergence.

3.2 Finite Element Analysis

Finite element analyses using a commercial computer code ANSYS 5.5[13] are performed to verify the analytical results for the theoretical study. The finite element method results are used as the baseline data. Three-dimensional model is constructed for the finite

Table 1 Dimensions and material properties

	Unit	Shell		Fluid
		Inner	Outer	
Length	m	0.300	0.300	
Mean radius	m	0.100	0.130	
Thickness	m	0.002	0.002	
Young's modulus	Pa	69E9	69E9	
Poisson's ratio		0.3	0.3	
Density	kg/m^3	2700	2700	1000
Sound speed	m/sec			1483
Bulk modulus of elasticity	Pa			2.2E9

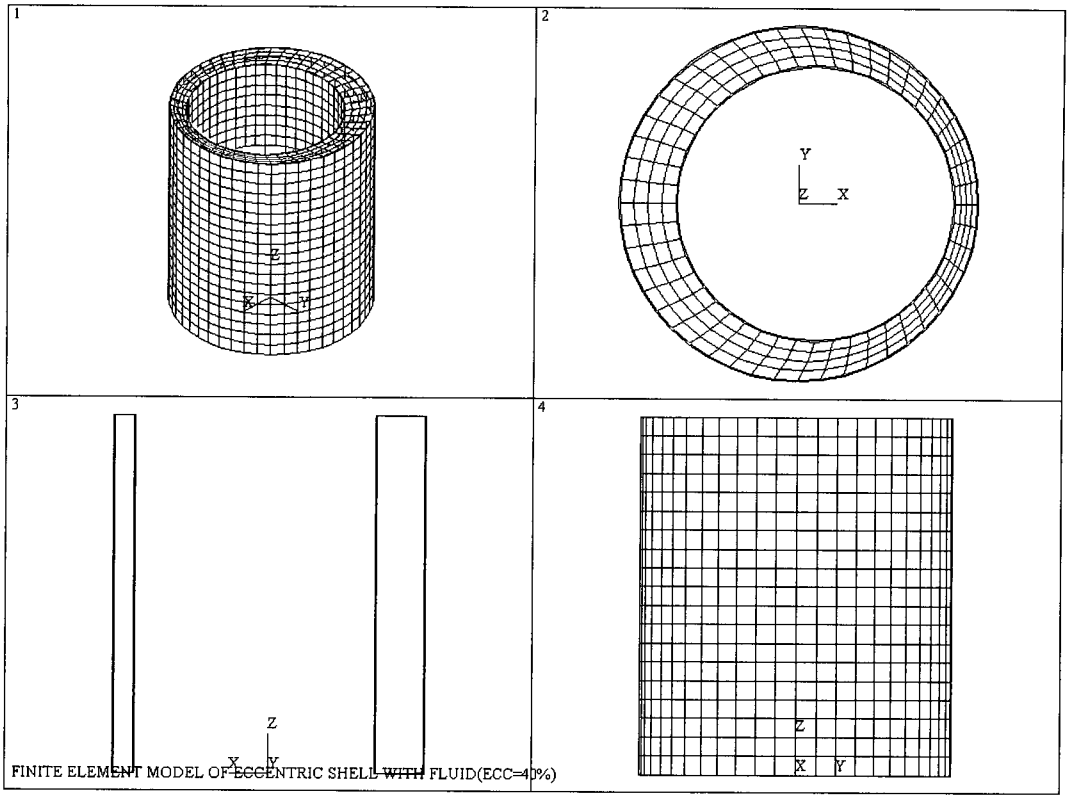

Fig. 2 Finite element model of cylindrical shells with fluid-filled annulus

element analysis. The fluid region is divided into a number of identical 3-dimensional contained fluid elements (FLUID80) with eight nodes having three degrees of freedom at each node. The fluid element FLUID80 is particularly well suited for calculating hydrostatic pressures and fluid/solid interactions. The circular cylindrical shell is modeled as elastic shell elements (SHELL63) with four nodes. The model has 3840 (radially 4 axially 20 circumferentially 48) fluid elements and 1920 shell elements as shown in Fig. 2.

The fluid boundary conditions at the top and bottom of the tank are zero displacement and rotation. The nodes connected entirely by the fluid elements are free to move arbitrarily in three-dimensional space, with the exception of those, which are restricted to motion in the bottom and top surfaces of the fluid cavity. The radial velocities of the fluid nodes along the wetted shell surfaces coincide with the corresponding velocities of the shells. Clamped-clamped boundary conditions at both ends are considered for the inner shell. The outer shell is considered to be rigid with zero displacement and rotation.

Sufficient number of master degree of freedoms is selected to calculate 200 frequencies and the reduced method is used for the eigenvalue and eigenvector extractions, which employ the Householder-Bisection-Inverse iteration extraction technique.

4. Results and Discussion

Mode shapes of the fluid-coupled shells are obtained by the finite element method and typical modes are plotted in Fig. 3, which shows the deformed mode shape of the fluid and shell elements for the modes of (1, 3), (2, 4), (3, 5) and (4, 5).

The frequency comparisons between analytical solution developed here and finite element method are shown in Fig. 4 and Table 2 for the eccentricity = 0 %. The discrepancy is defined as

$$\text{Discrepancy}(\%) = \frac{\text{frequency by FEM - theoretical frequency}}{\text{frequency by FEM}} \times 100 \quad (31)$$

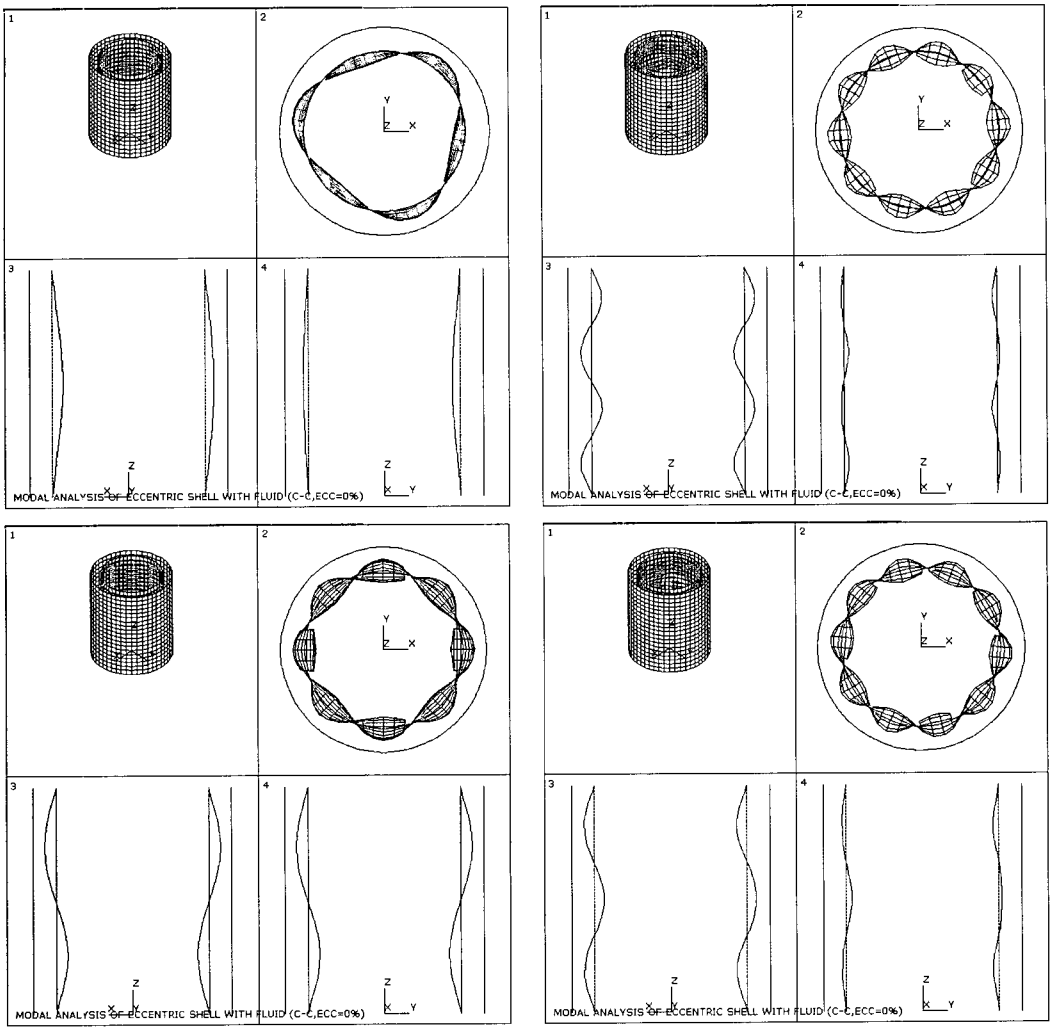

Fig. 3 Typical mode shapes for eccentricity = 0 %

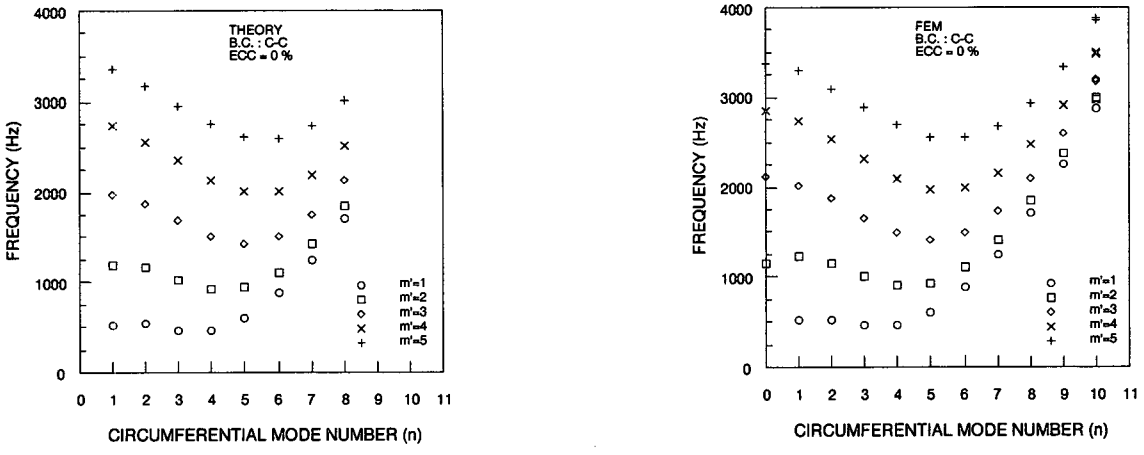

Fig. 4 Frequency comparisons for eccentricity = 0%

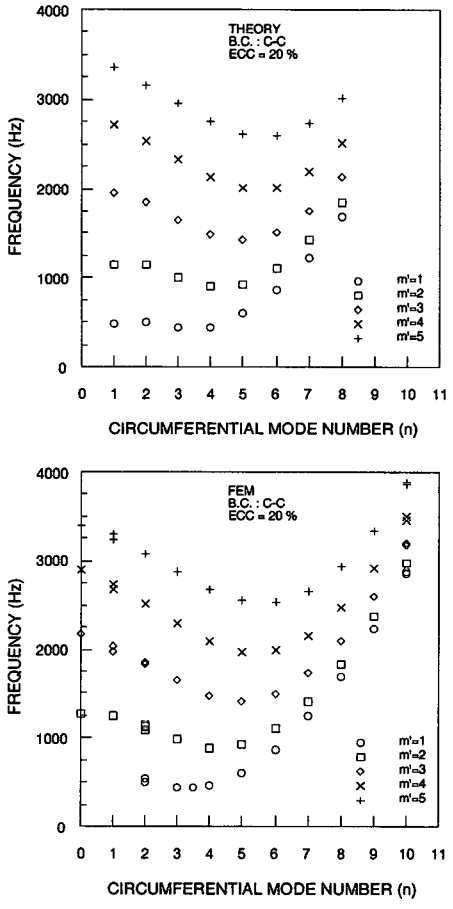

Fig. 5 Frequency comparisons for eccentricity = 20%

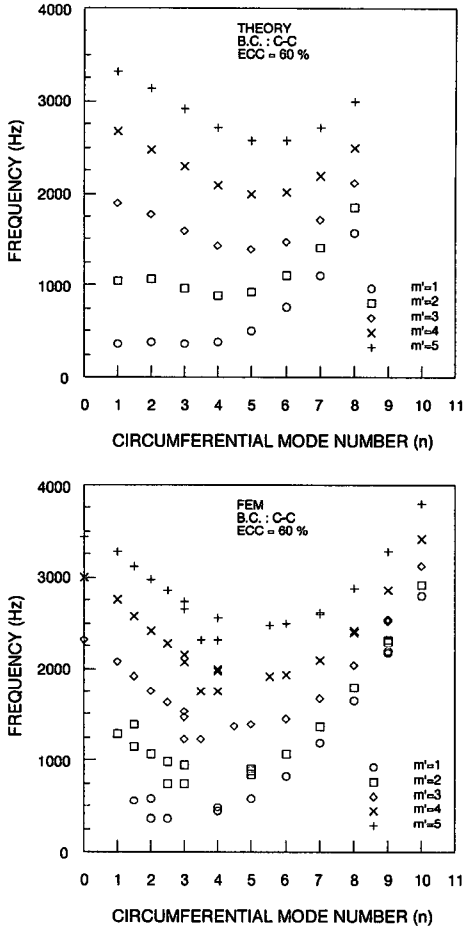

Fig. 6 Frequency comparisons for eccentricity = 40%

The largest discrepancy between the theoretical and finite element analysis results is 2.7 % for the mode of (1, 2). Discrepancies defined by equation (31) are always less than 3 %, therefore the theoretical results agree well with finite element analysis results, verifying the validity of the analytical method developed.

Frequency comparisons for the eccentricity of 20 % are shown in Fig. 5. Not like the case of the 0 % eccentricity, there are several points to be noted. No (1, 1) mode appeared in the finite element analysis and also modes of (2, 1), (1, 2) and (2, 2) have rather large discrepancies even though they are within 10 %. This is because (1, 1) mode for 0% eccentricity tends to move to adjacent modes such as (1, 2) or (2, 1) for the case of the 20 % eccentricity. Also, (1, 3.5) mode of 445 Hz appeared, which is in progress of moving from (1, 3) to (1, 4) modes. This kind of trend is more evident as eccentricity becomes larger as shown in Fig. 6 and 7 for the eccentricities of 40 % and 60 %, respectively.

The variation of mode shapes with respect to eccentricity for axial mode $m'=1$ is shown for the first 12 modes in Fig. 8, which shows that some modes move to another modes with the change of eccentricity. For example one pair of (1, 4) mode appeared in the eccentricity of 40 % or less, but there are two pairs of (1, 4) modes in the eccentricity of 60 %; one is the original (1, 4) mode and the other is the mode from (1, 3) of 40 % eccentricity. Also, two pairs of (1, 2) modes appeared in the eccentricity of 20 %; one is original (1, 2) mode and the other is the mode from (1, 2) mode of the 0 % eccentricity. This kind of mode movement with larger eccentricity is the cause of the appearance of several circumferential mode number of order 0.5, and also the reason for not appearing of several modes such as (1, 1) mode for eccentricities of 20 % and (2, 4) mode for eccentricities of 60 %.

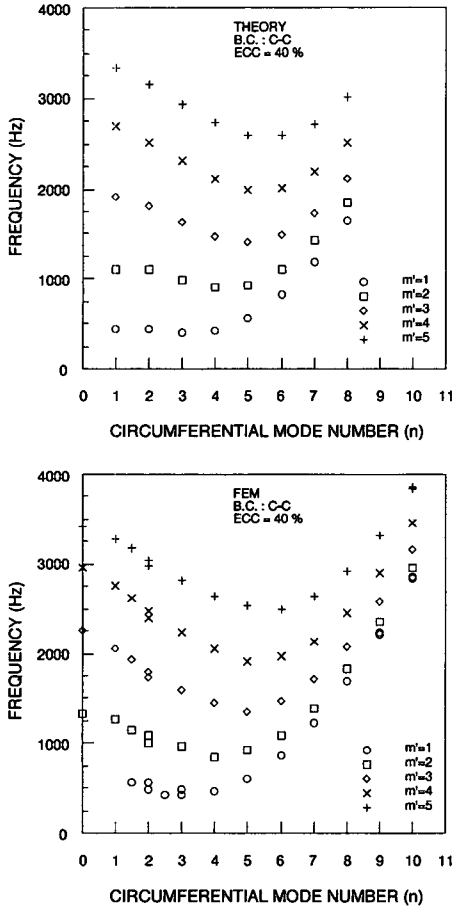

Fig. 7 Frequency comparisons for eccentricity = 60%

Because there is unsymmetric configuration for shells with eccentricity, there should be unsymmetric modes for certain modes. This trend is much more severe with large eccentricity except for circumferential and/or axial modes. Two separate values of mode are obtained especially for axial mode number $n \leq 2$ in eccentricity = 20 %, $n \leq 3$ in eccentricity = 40 % and $n \leq 5$ in eccentricity = 60 %. Contrary to this, modes for the eccentricity = 0 % have exactly the same symmetric mode shapes for all modes as shown in Fig. 9.

Fig. 10 shows the variation of frequency values with respect to the eccentricity for several modes which are not much affected by the eccentricity. If there is no movement of modes with increasing eccentricity, the effect of eccentricity on the frequencies is almost negligible, which is especially true for the high circumferential modes. Therefore the eccentricity is found to be more effective on the separation of modes or mode movement from lower to higher circumferential modes than on the change of the frequencies.

Table 2 Natural frequencies for eccentricity = 0%

Circumferential mode(n)	Axial mode(m')	Frequency(Hz)		Discrepancy (%)
		Theory	FEM	
1	1	533	528	-0.95
	2	1195	1221	2.13
	3	1975	2015	1.99
	4	2744	2738	-0.22
	5	3362	3289	-2.22
2	1	535	521	-2.69
	2	1163	1150	-1.13
	3	1872	1868	-2.14
	4	2545	2539	-2.36
	5	3177	3101	-2.45
3	1	469	459	-2.18
	2	1021	1004	-1.69
	3	1680	1659	-1.27
	4	2344	2308	-1.56
	5	2962	2888	-2.56
4	1	471	465	-1.29
	2	919	908	-1.21
	3	1503	1484	-1.28
	4	2132	2098	-1.62
	5	2754	2689	-2.42
5	1	612	607	-0.82
	2	937	928	-0.10
	3	1429	1414	-1.06
	4	2005	1976	-1.47
	5	2614	2560	-2.11
6	1	880	876	-0.05
	2	1111	1102	-0.08
	3	1507	1491	-1.07
	4	2018	1988	-1.51
	5	2596	2544	-2.04
7	1	1249	1246	-0.02
	2	1427	1416	-0.08
	3	1747	1726	-1.22
	4	2192	2154	-1.76
	5	2729	266/8	-2.29
8	1	1707	1704	-0.18
	2	1858	1844	-0.08
	3	2130	2100	-1.43
	4	2520	2471	-1.98
	5	3017	2938	-2.69

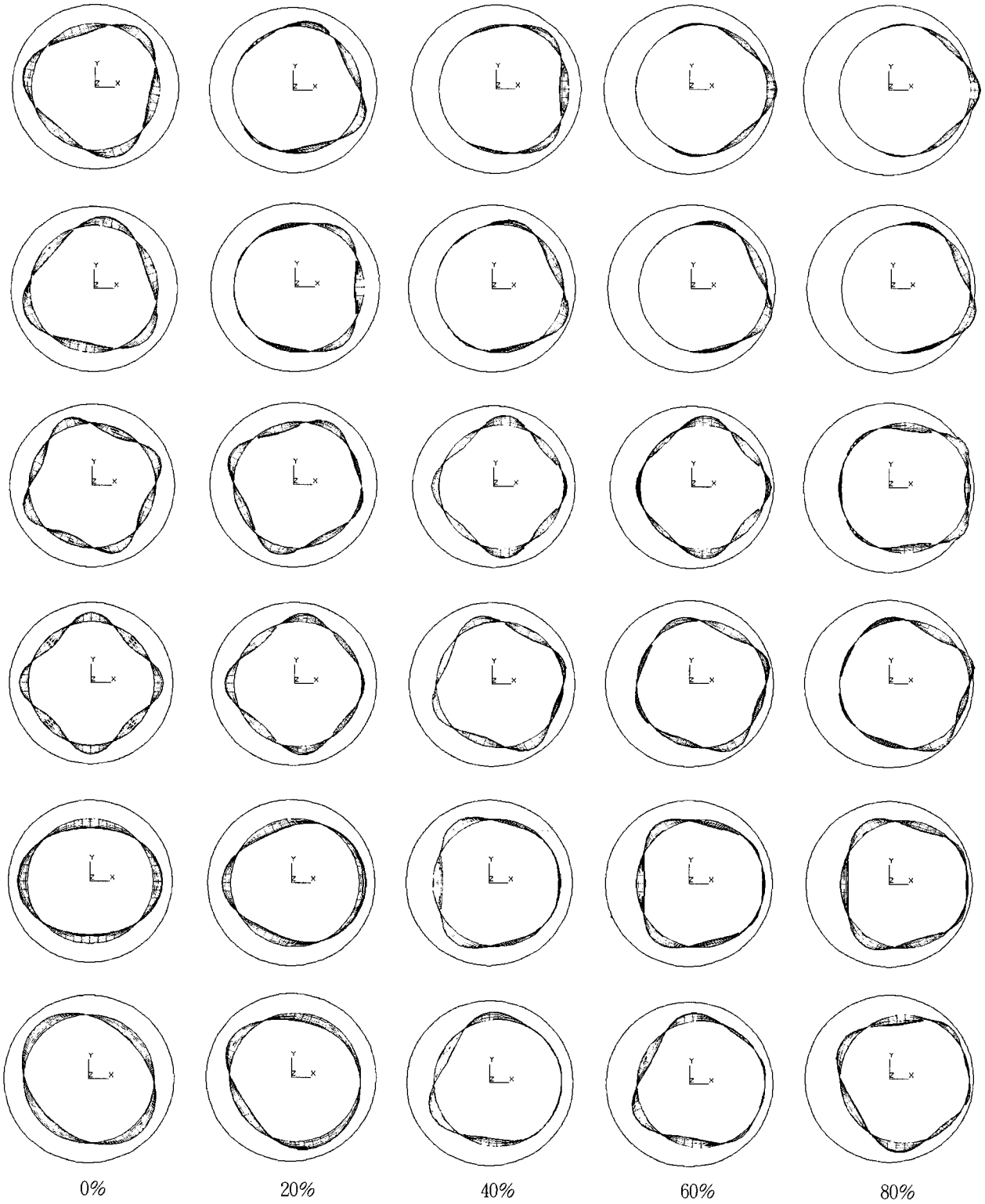

Fig. 8 Variation of mode shapes for $m=1$ with respect to eccentricity

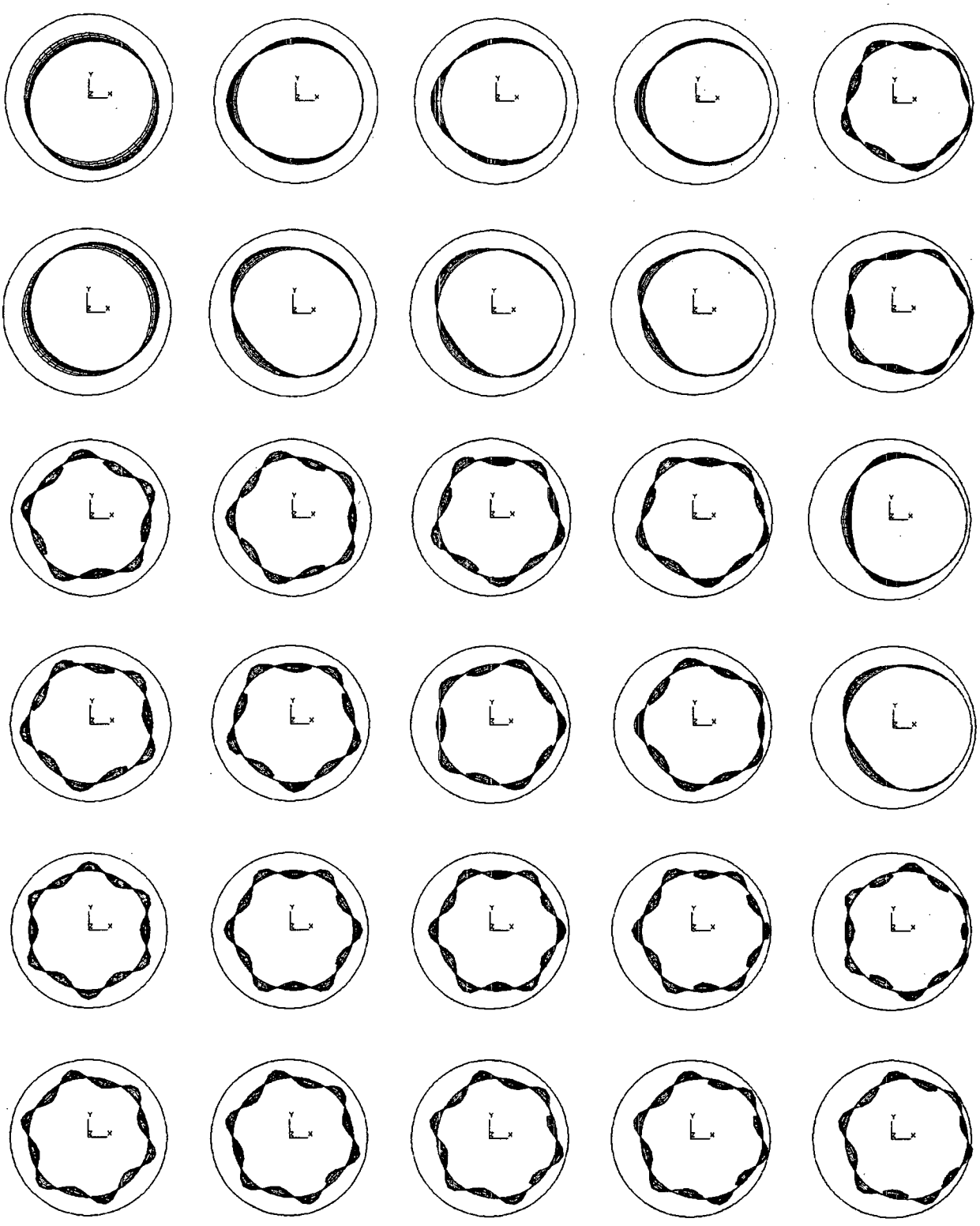

Fig. 8 Variation of mode shapes for $m'=1$ with respect to eccentricity (Cont'd)

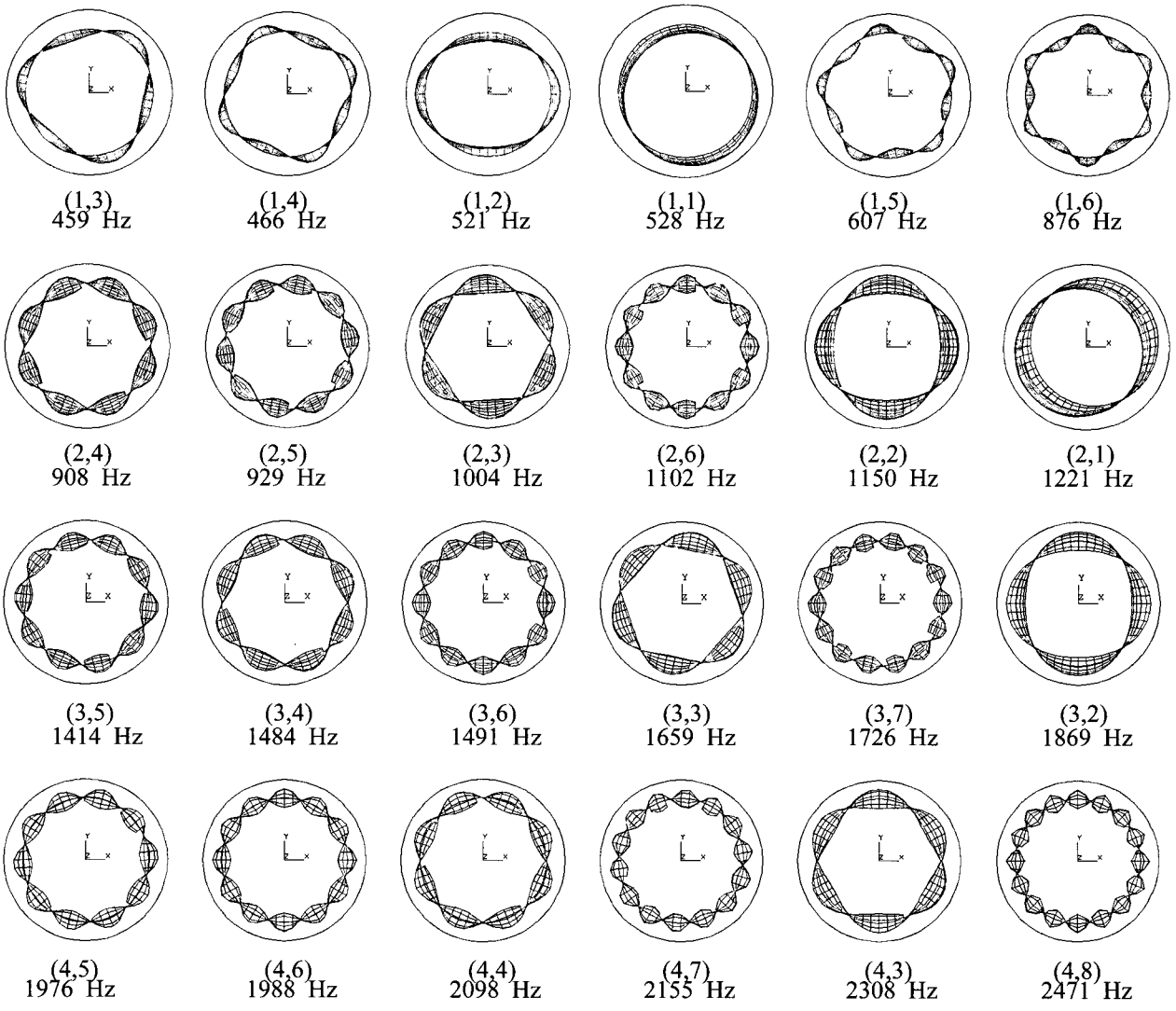

Fig. 9 Mode shapes for eccentricity = 0%

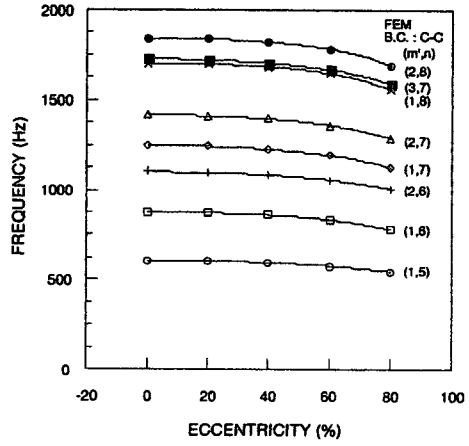

Fig. 10 Variation of frequencies with respect to eccentricity

5. Conclusions

An analytical method to estimate the coupled frequencies of the cylindrical shells with fluid-filled annulus is developed using the series expansion method based on the Fourier transformation. To verify the validity of the analytical method developed, finite element method is used and the frequency comparisons between them are found to be in good agreement, especially for the eccentricity of 0 %. With the increasing eccentricity some modes are separated or mode movement are found, which is not incorporated in the theoretical development. This needs to be studied in the future to define more sophisticated modes such as the circumferential mode of

order 0.5. But in general the theory developed agrees well with the finite element method except for several transition modes which are changing with eccentricity. The effect of the eccentricity on the frequencies is found to be more severe on the appearance of transition modes or disappearance of certain modes rather than on the frequency changes. Therefore it is recommended to investigate the modal characteristics rather than frequency itself to know that how much eccentricity is there in the shells with fluid-filled annulus.

References

(1) Song, S. H., Jhung, M. J., 1999, "Experimental Modal Analysis on the Core Support Barrel of Reactor Internals Using a Scale Model," KSME International Journal, Vol.13, No. 8, pp.585~594.

(2) Jhung, M. J., 1996, "Shell Response of Core Barrel for Tributary Pipe Break," International Journal of Pressure Vessels and Piping, Vol. 69, No.2, pp.175~183.

(3) Chen, S. S., Rosenberg, G. S., 1975, "Dynamics of a Coupled Shell-fluid System," Nuclear Engineering and Design, Vol. 32, pp.302~310.

(4) Yoshikawa, S., Williams, E. G., Washburn, K. B., 1994, "Vibration of Two Concentric Submerged Cylindrical Shells Coupled by the Entrained Fluid," Journal of Acoustic Society of America, Vol. 95, pp.327 3~3286.

(5) Jhung, M. J., et al., 2000, "Modal Analysis of Coaxial Shells with Fluid-Filled Annulus," Journal of the Korean Nuclear Society, Vol.32, No.4; (to appear).

(6) Danila, E. B., Conoir, J. M. and Izbicki, J. L., 1995, "The Generalized Debye Series Expansion : Treatment of the Concentric and Non-concentric Cylindrical Fluid-fluid Interfaces," Journal of the Acoustical Society of America, Vol. 98, pp.3326~3342.

(7) Jeong, K. H., Lee, S. C., 1996, "Fourier Series Expansion Method for Free Vibration Analysis of Either a Partially Fluid-filled or a Partially Fluid-surrounded Circular Cylindrical Shell," Computers & Structures, Vol. 58, pp.937~946.

(8) Jeong, K. H., 1998, "Natural Frequencies and Mode Shapes of Two Coaxial Cylindrical Shells Coupled with Bounded Compressible Fluid," Journal of Sound and Vibration, Vol. 215, pp.105~124.

(9) Chung, H., 1981, "Free Vibration Analysis of Circular Cylindrical Shells," Journal of Sound and Vibration, Vol. 74, pp.331~350

(10) Jeong, K.H., Kim, K.J., 1998, "Free Vibration of a Circular Cylindrical Shell Filled with Bounded Compressible Fluid," Journal of Sound and Vibration Vol. 217, pp.197~221.

(11) Sneddon, N., 1951, Fourier Transforms, McGraw-Hill Book, New York.

(12) Watson, G.N., 1980, A Treatise on the Theory of Bessel Functions, Second Edition, Cambridge University Press, Cambridge.

(13) ANSYS, 1998, ANSYS Structural Analysis Guide, ANSYS, Inc., Houston.